FORSCHUNGSZENTRUM ROSSENDORF FZR

WISSENSCHAFTLICH-TECHNISCHE BERICHTE
FZR-292
April 2000
ISSN 1437-322X

Eberhard Altstadt und Hans-Georg Willschütz

Development of an Integral Finite Element Model for the Simulation of Scaled Core-Meltdown-Experiments

Herausgeber:
FORSCHUNGSZENTRUM ROSSENDORF
Postfach 51 01 19
D-01314 Dresden
Telefon +49 351 26 00
Telefax +49 351 2 69 04 61
http://www.fz-rossendorf.de/

Als Manuskript gedruckt

FORSCHUNGSZENTRUM ROSSENDORF
WISSENSCHAFTLICH-TECHNISCHE BERICHTE
FZR-292
April 2000

Eberhard Altstadt und Hans-Georg Willschütz

Development of an Integral Finite Element Model for the Simulation of Scaled Core-Meltdown-Experiments

Abstract

To get an improved understanding and knowledge of the processes and phenomena during the late phase of a core melt down accident the FOREVER-experiments (Failure Of REactor VEssel Retention) are currently underway. These experiments are simulating the lower head of a reactor pressure vessel under the load of a melt pool with internal heat sources. The geometrical scale of the experiments is 1:10 compared to a common Light Water Reactor. During the first series of experiments the creep behaviour of the vessel is investigated.
Due to the multi-axial creep deformation of the three-dimensional vessel with a non-uniform temperature field these experiments are on the one hand an excellent possibility to validate numerical creep models which are developed on the basis of uniaxial creep tests. On the other hand the results of pre-test calculations can be used for an optimized experimental procedure.
Therefore a Finite Element model is developed on the basis of the multi-purpose commercial code ANSYS/Multiphysics®. Using the Computational Fluid Dynamic module the temperature field within the vessel wall is evaluated. The transient structural mechanical calculations are performed applying a creep model which is able to take into account great temperature, stress and strain variations within the model domain. The new numerical approach avoids the use of a single creep law with constants evaluated for a limited stress and temperature range. Instead of this a three-dimensional array is developed where the creep strain rate is evaluated according to the actual total strain, temperature and equivalent stress for each element.
Performing post-test calculations for the FOREVER-C2 experiment it was found that the assessment of the experimental data and of the numerical results has to be done very carefully. Because of the accelerating creep strain rate after pressurization, the recorded creep process appears to be tertiary, if a constant temperature field is assumed. But a slight temperature increase during the creep deformation stage of the experiment could explain the observed creep behaviour, too.
Taking into account both - experimental and numerical results - gives a good opportunity to improve the simulation and understanding of real accident scenarios.

Acknowledgements

The authors are greatful to Th. Moessner (Rossendorf) who supported the programming work for the customized ANSYS code. The FOREVER C1 experiment was performed under the partial sponsorship of EU. The FOREVER C2 experiment was performed under the sponsorship of the APRI Project of the SKI, Swedish and Finish Power Companies, USNRC, and HSK.

Contents

Nomenclature

Latin

a	thermal diffusivity	[m^2/s]
c	creep model constant	[-]
C	CFD-model constant	[-]
D	damage parameter	[-]
e	emissivity	[-]
g	gravitational acceleration	[m/s^2]
k	turbulent kinetic energy	[m^2/s^2]
P	pressure	[Pa]; [bar]
q	volumetric heat generation	[W/m^3]
Q	total heat generation	[W]; [VA]
r	radius	[m]
Ra	Rayleigh-number	[-]
s	wall thickness	[m]
t	time	[s]
T	temperature	[°C]; [K]
u,v,w	velocities	[m/s]
U	displacement	[m]
W	weighting factor	[-]
x	horizontal (radial) coordinate	[m]
y	vertical (axial) coordinate	[m]
z	coordinate	[m]

Greek

β	coefficient of thermal expansion	[1/K]
ε	strain	[-]
ε	turbulent kinetic energy dissipation rate	[m^2/s^3]
Θ	azimuthal angle	[°]
λ	heat conductivity	[W/mK]
μ	dynamic viscosity	[kg/ms]
ν	kinematic viscosity	[m^2/s]
ρ	density	[kg/m^3]
σ	stress	[Pa]
σ	model constant	[-]
Φ	viscous dissipation	[W/m^3]

Indices

a	after
amb	ambient
b	before
c	circumferential
cr	creep
eqv	equivalent
frac	fracture, rupture
H	high
i	inner, internal
L	low
max	maximal
min	minimal
r	radial
s	solidus
steel	steel
sum	summation, total
t	turbulent
v	vertical
V	volumetric
x	horizontal, radial
y	vertical

Abbreviations

C	Creep
CFD	Computational Fluid Dynamics
FE	Finite Element
FEM	Finite Element Method
FOREVER	Failure Of REactor VEssel Retention
LDT	Linear Displacement Transducer
LWR	Light Water Reactor
RPV	Reactor Pressure Vessel
TC	ThermoCouple
UPF	User Programmable Feature

1 Introduction

For future nuclear power plants it is demanded that there are no consequences for the environment and the population even in the closest vicinity of the plant during, and after, any conceivable accident scenario. This includes the hypothetical scenario of a severe accident with subsequent core meltdown and formation of a melt pool in the lower plenum of the reactor pressure vessel (RPV) of a Light Water Reactor (LWR). One accident management strategy is to stabilize the in-vessel debris configuration in the RPV and use that as the major barrier against uncontrolled release of heat and radionuclides into the containment. This strategy also applies to existing plants.

To obtain an improved understanding and knowledge of the melt pool convection and the timing and mode of the vessel creep failure during the late phase of a core melt down accident the FOREVER-experiments (Failure Of REactor VEssel Retention) are currently underway at the Division of Nuclear Power Safety of the Royal Institute of Technology Stockholm (Sehgal et al., 1999).

These experiments are simulating the behaviour of the lower head of the RPV under the thermal loads of a convecting melt pool with decay heating, and under the pressure loads that the vessel may suffer in a depressurization scenario. The geometrical scale of the experiments is 1:10 compared to a common Light Water Reactor.

The FOREVER program consists of three major phases. During the first series of experiments the creep behaviour and failure (FOREVER-C) of the vessel under the attack of the melt pool and an internal pressure load is investigated. It is intended to maintain the creep process until vessel failure.

Due to the multi axial creep deformation of the vessel with a non-uniform temperature field these experiments are on the one hand an excellent source of data to validate creep models for pressure vessel steels which are developed on the basis of uniaxial creep tests. On the other hand the results of pre-test calculations can be used to optimize the experimental procedure with considerations of the uncertainties in the applied models and assumed boundary conditions. Therefore, a two-dimensional Finite Element (FE) model is developed, based on the multi-purpose code ANSYS/ Multiphysics® at the Institute of Safety Research at the Forschungszentrum Rossendorf, Dresden, Germany. Using the Computational Fluid Dynamics (CFD) module the temperature field within the melt pool and within the vessel wall is evaluated. The transient structural mechanical calculations are, then, performed applying a creep model which takes into account large temperature, stress and strain variations.

This numerical approach avoids the use of a single creep law (e.g. strain hardening model) with parameters evaluated from a limited stress and temperature range. Instead of this strain rate - strain relations can be applied which are separately fitted for different temperature and stress levels.

Performing post-test calculations for the FOREVER-C2 experiment it was found that the comparison of the experimental data with the predicted numerical results has to be done carefully. On the one hand measured data on melt pool temperature was quite meager during the late phase of the experiment when many thermocouples, at high temperature locations, failed. On the other hand the calculated results for the creep process show great sensitivity to small

changes in the temperature and structure-mechanical boundary conditions. For example in the experiment an increasing creep strain rate was observed. The numerical simulation shows that this accelerated creep could be due to a slight temperature increase rather than to the tertiary creep phase. Taking into account both - experimental and numerical results - provides a good opportunity to improve the simulation and the understanding of the vessel failure mechanisms. Of particular interest are (i) the time to failure and (ii) the location and mode of failure.

2 Experimental Setup and First Results

In **Figure 1** the principal setup of the FOREVER C-experiments is shown (Sehgal et al., 1999). Due to the limitation of the heating power (Q_{max}=22kW) in the C1-experiment the temperature at the outer vessel surface was below 800°C at the beginning of the pressurization phase and decreasing during the creep deformation stage. Therefore the creep strain was limited. In the experiment C2 much higher creep strains were reached due to increased power input (Q_{max}>40kW) and external temperatures of close to 1000°C were observed in the hot focus region at the upper hemispherical part. The analysis presented in this work is based on the latter experiment.

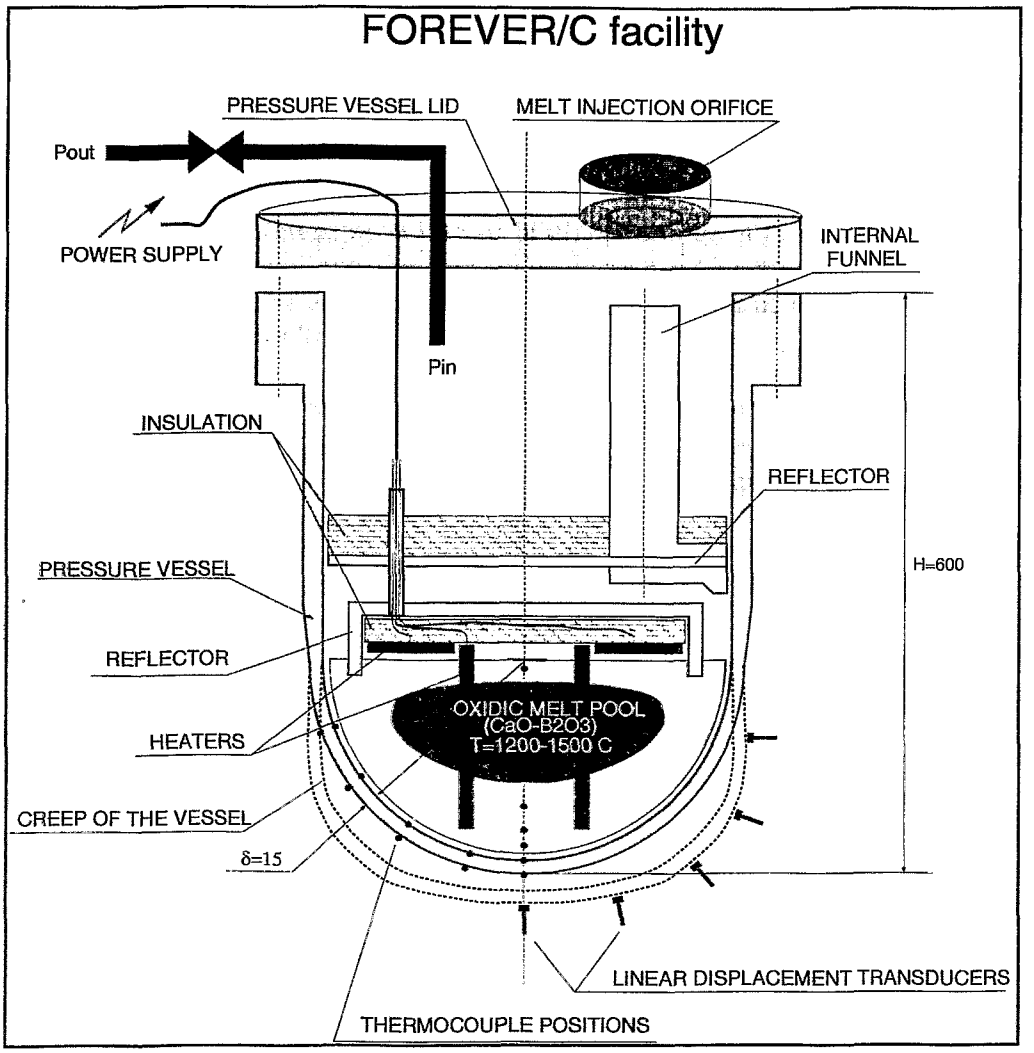

Figure 1: Principal scheme of the FOREVER-Creep tests. Scheme is not to scale.

The hemispherical and the cylindrical part of the vessel have, in principal, inner radii of r_i=188mm. The wall-thickness of the cylindrical part which was made of German 15Mo3 RPV steel was s=16.0mm. The hemisphere had a designed wall thickness of s=15.0mm and was made of French 16MND5 RPV steel. Due to the hot-pressing manufacturing of the hemisphere from a plate the wall thickness varied in azimuthal and circumferential direction. A second point to be kept in mind is that the melt was prepared outside the vessel and poured through an

internal funnel to one side of the vessel (cf. **Fig. 1**). It can be assumed that these two factors caused some 3D-bending process resulting in a horizontal movement before and during the creep process of the bottom center of the hemisphere which should only relocate in vertical direction presuming ideal symmetry conditions.

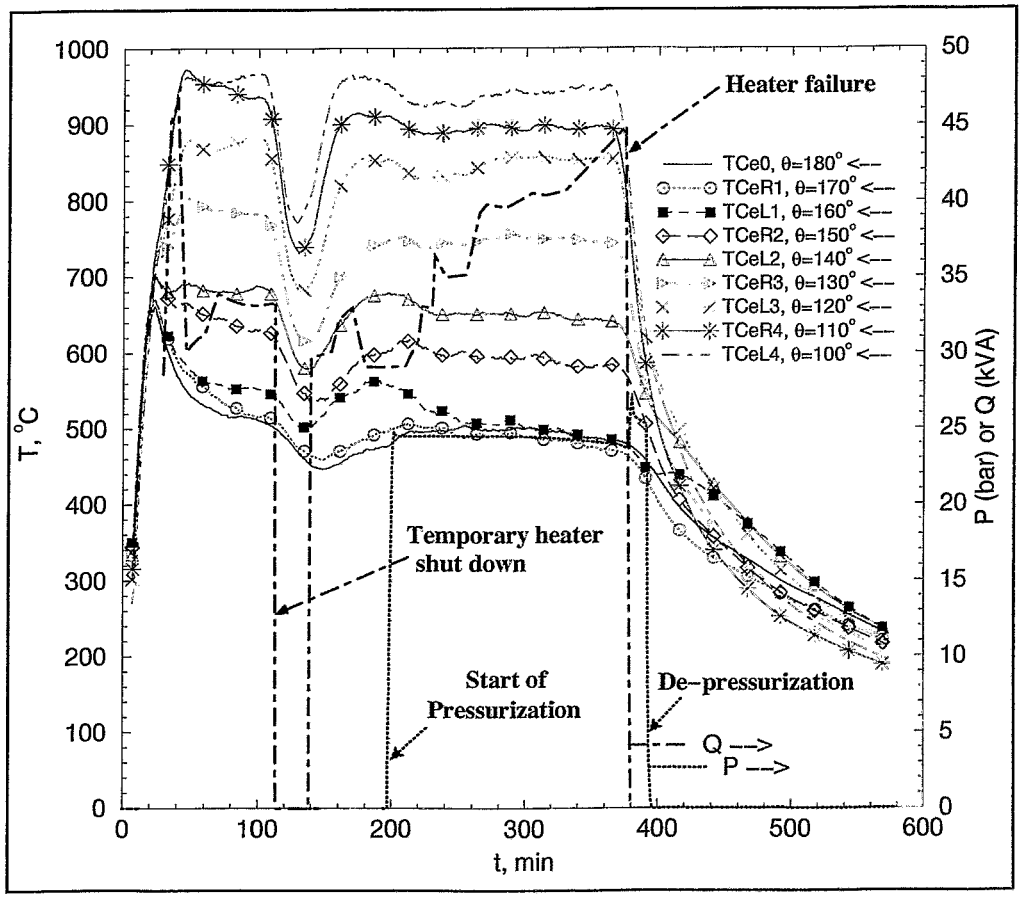

Figure 2: General course of the experiment C2: power input Q / [kVA], pressure P / [bar] and external temperatures T / [°C]. $\Theta = 180°$ refers to the very bottom of the hemispherical bottom head.

The oxidic melt employed as a simulant for the prototypic UO_2-ZrO_2-Zr melt was a CaO-B_2O_3 mixture (30-70 wt.-%) which has a solidus temperature of T_s=1250K and is a rather aggressive oxide, especially at high temperatures. To model the internal decay heat generation specially designed heater rods fixed to an internal insulation-reflector-lid were immersed into the melt from the top. The lid was fixed to the upper part of the vessel. After melt was poured the melt injection orifice in the vessel lid was closed and the vessel inside could be pressurized by Argon. The FOREVER experiments are performed in a containment. The total duration of the experiment C2 was nearly 10 hours from the start of pre-heating the vessel to the stop of the data recording at the end of the cooldown stage.

Figure 2 shows the time history of the heating power input Q, the internal pressure P and the temperatures at different azimuthal locations of the hemisphere. The angle Θ refers to the global spherical coordinate system located in the center of the hemisphere where $\Theta = 0°$ denotes the vertical upward direction, i. e. $\Theta = 180°$ denotes the very bottom of the vessel.

Until melt pouring (t=25-30min) all thermocouples show the same temperature. After some 120 min there was a temporarily heater shut down to install additional cooling units to the power supply cables. With the re-gained power supply and temperature level the system was pressurized at t=200min.

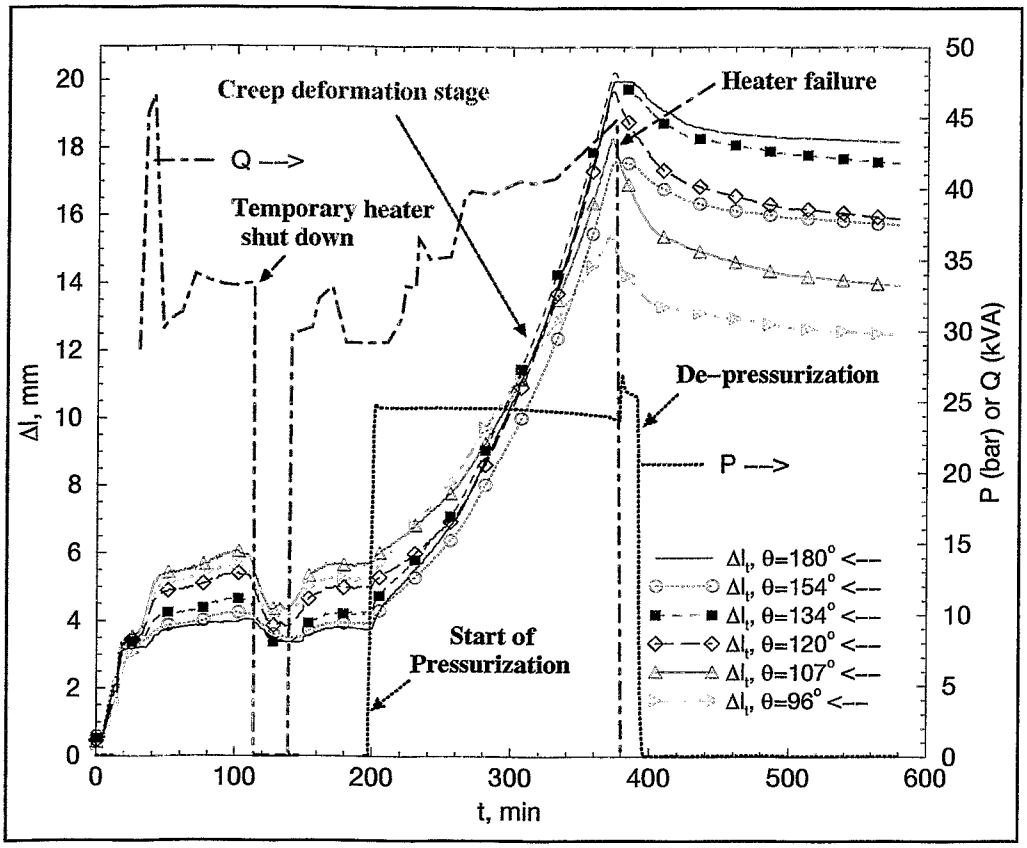

Figure 3: General course of the experiment C2: power input Q / [kVA], pressure P / [bar] and total displacement U_{sum} / [mm] at different external positions of the hemisphere. $\Theta = 180°$ refers to the very bottom of the hemispherical bottom head.

In **Figure 3** the total displacement U_{sum} at different positions of the external vessel surface during the course of the experiment is shown. The thermal expansion of the vessel due to the hot melt pool can be seen clearly. The start of the pressurization indicates the beginning of the creep deformation stage. The creep curves show an acceleration of the creep strain which indicates normally tertiary creep, because primary creep curves show a declining strain rate and secondary creep is characterized by a constant creep strain rate. As the names indicate the three creep stages should occur in this sequence. And this behaviour was observed in FOREVER-C1. So far the reason for the observations in C2 is not exactly known. Due to the creep expansion of the vessel the volume of the hemisphere is increasing to the third power of the increase of the radius. This causes a decreasing melt level and as a consequence in the experiment C2 the uppermost parts of the heater rods were no longer immersed in the pool. Therefore they burned by overheat and the power supply was stopped. Thus, the experiment could not be run until vessel failure. The thermal contraction after heater failure is also visible in **Figure 3.**

For more detailed description and for scaling considerations of the experimental setup the reader is referred to Sehgal et al. (1999).

3 Thermo-Fluid-Dynamic Model and Results

For the evaluation of the temperature field within the vessel wall the CFD-module FLOTRAN® of the FE-code ANSYS® is used. A 2D-axis-symmetric model with appropriate boundary conditions and material properties is developed.

A pure homogenous melt pool is assumed inside the vessel with the surface level set to the welding joint between hemisphere and cylinder. **Figure 4** shows the FE-mesh and the thermal boundary conditions. The mesh consists of 1740 elements with 1400 of them belonging to the liquid region at the beginning of the calculation. Due to some prior estimations it was found that the main heat transfer mechanism at the model boundaries is radiation. Therefore at the vessel outside an radiative heat transfer boundary condition is applied with an ambient temperature of T_{amb}=400K. During the experiment the external vessel wall was subject to strong oxidization. Owing to the lack of exact steel surface emissivities under these conditions a surface emissivity of e_{steel}=0.8 has been used. In fact the emissivity could have been higher, but the chosen value can be considered as appropriate (VDI, 1994; Sala 1984, James and Lord, 1992). Also for the internal surfaces radiative boundary conditions have been modelled: between insulation and melt pool (cf. **Fig. 1**) T_{amb} was set to 1200K, above insulation it was 800K. The emissivity was the same as on the outside. Of course this is a simple model which has to be improved, but the results show that it works quite satisfactorily for a first attempt. In the experiment the heat is released at the discrete positions of the heater rods. In the model a homogenous volumetric heat source is assumed which is applied to the volume within which the heaters are to be found. Especially at the very bottom the distance between the heater and the vessel wall has a significant influence on the crust formation, which will be considered later (cf. **Fig 4**). The internal Rayleigh number can be employed to assess the idealized configuration:

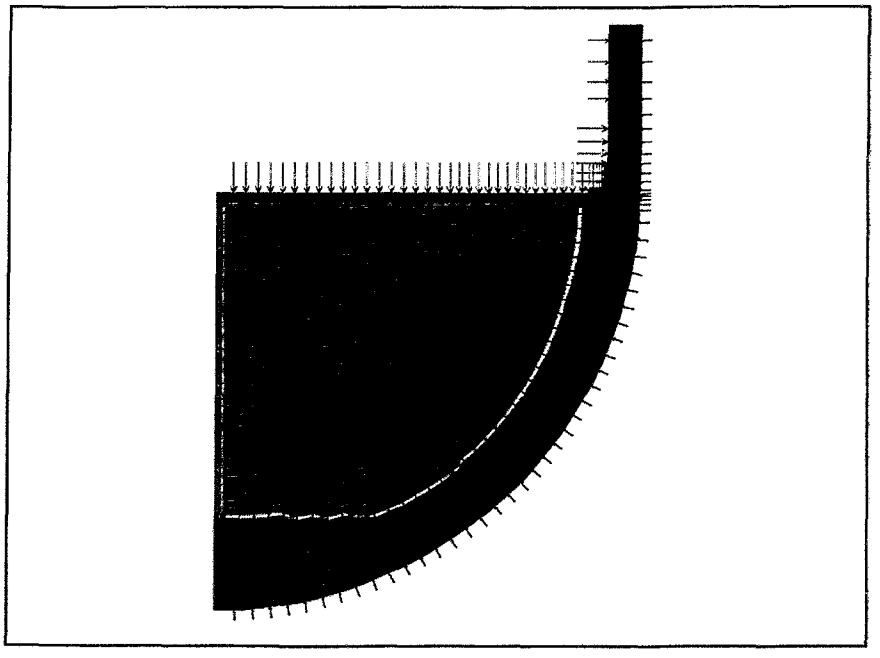

Figure 4: Axis-symmetric 2D-thermo-fluid-dynamic FE-Model of the FOREVER-C2-experiment. Red coloured area indicates volumetrical heat generation zone. Length and colour of arrows corresponds to the applied ambient temperature for radiative heat transfer boundary condition. Cylindrical part is not fully shown.

$$Ra_i = \frac{g\beta q_v r_i^5}{\nu a \lambda} \qquad (1)$$

With the applied power range, the melt properties employed and the assumptions made above, the internal Rayleigh number for this configuration is calculated in a range of $Ra_i=0.5\ 10^{10}$ to $Ra_i=1.0\ 10^{10}$. Concerning the modelling approach this Rayleigh number seems to be small enough (Sehgal et al., 1996) to model the heat transfer within the pool by the application of a standard-k-ε-turbulence model which is provided by FLOTRAN®.
The well-known equation for the turbulent kinetic energy k in 3D Cartesian coordinates is:

$$\frac{\partial \rho k}{\partial t} + \frac{\partial \rho u k}{\partial x} + \frac{\partial \rho v k}{\partial y} + \frac{\partial \rho w k}{\partial z} =$$
$$\frac{\partial}{\partial x}\left(\frac{\mu_t}{\sigma_k}\frac{\partial k}{\partial x}\right) + \frac{\partial}{\partial y}\left(\frac{\mu_t}{\sigma_k}\frac{\partial k}{\partial y}\right) + \frac{\partial}{\partial z}\left(\frac{\mu_t}{\sigma_k}\frac{\partial k}{\partial y}\right) \qquad (2)$$
$$+\Phi - \rho\varepsilon + \frac{C_4 \beta \mu_t}{\sigma_k} g \frac{\partial T}{\partial z}$$

And the equation for the turbulent dissipation rate ε is:

$$\frac{\partial \rho \varepsilon}{\partial t} + \frac{\partial (\rho u \varepsilon)}{\partial x} + \frac{\partial (\rho v \varepsilon)}{\partial y} + \frac{\partial (\rho w \varepsilon)}{\partial z} =$$
$$\frac{\partial}{\partial x}\left(\frac{\mu_t}{\sigma_\varepsilon}\frac{\partial \varepsilon}{\partial x}\right) + \frac{\partial}{\partial y}\left(\frac{\mu_t}{\sigma_\varepsilon}\frac{\partial \varepsilon}{\partial y}\right) + \frac{\partial}{\partial z}\left(\frac{\mu_t}{\sigma_\varepsilon}\frac{\partial \varepsilon}{\partial y}\right) \qquad (3)$$
$$+ C_{1\varepsilon}\frac{\varepsilon}{k}\Phi - C_2\rho\frac{\varepsilon^2}{k} + \frac{C_\mu (1 - C_3)\beta\rho k}{\sigma_t} g \frac{\partial T}{\partial z}$$

where Φ denotes the viscous dissipation term. The default values of ANSYS® for the model constants (σ_k, σ_ε, $C_{1\varepsilon}$, C_2, C_μ) are set according to those proposed by Launder and Spalding (1974). The final term in the equations (2) and (3) is used to model the effect of buoyancy. The default values of C_3 and C_μ are 1.0 and 0.0 respectively, that means there is no contribution due to buoyancy effects in turbulence modelling. To model the unstable stratification at the top in the FOREVER-experiment C_3 was set to 1.0 and C_μ to 0.5.

Assuming slow temperature changes in the vessel wall and in the lower part of the melt pool a dynamic crust is modelled by stopping the solution every 20 seconds and checking the temperature field. For those elements where the melt temperatures are below the solidus temperature of T_s=1250K at all nodes, the material number is changed so that these elements belong to the solid region of the oxidic crust. This approach has been chosen because in future calculations the oxidic crust has to be modelled structurally, too, to be able to model a gap formation between crust and vessel. **Figure 5** shows the computational domain with the different materials and the boundary conditions at the surface and at the symmetry line where the free slip condition is applied.

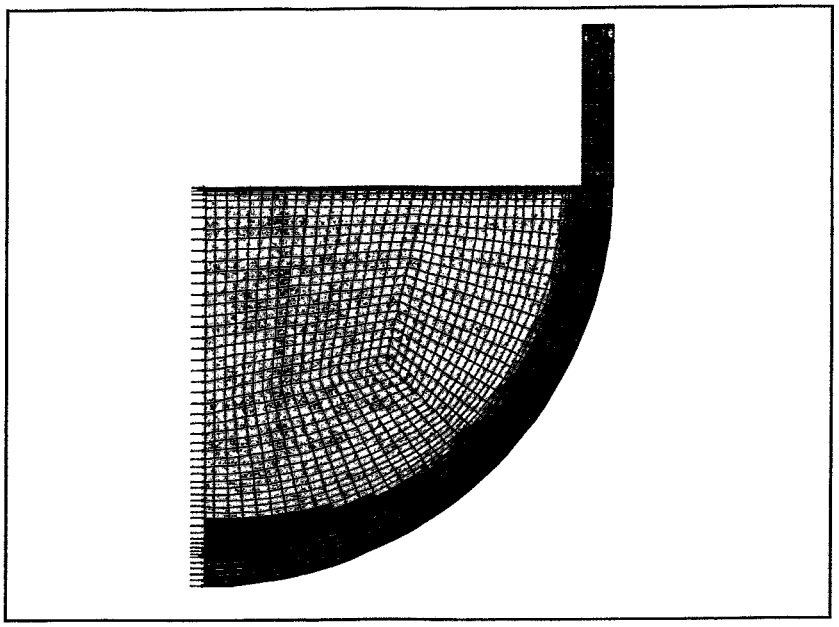

Figure 5: Mesh, fluid-dynamic boundary conditions and material definition of the CFD-model after reaching quasi-stationary state with input power Q=35kW and dynamic crust formation. Colours: magenta=solid steel, blue=solid oxidic crust, orange=liquid oxid. Cylindrical part is not fully shown.

So far different power inputs were modelled in transient calculations starting with homogenous initial temperatures within melt pool and vessel wall. The heat generation rates were chosen according to the experimental range which had changed from 30kW to 45kW (cf. **Figs. 2, 3**). In these calculations a thermal steady state for the vessel wall was observed after some 20-30min. In **Figure 6** the steady state temperature field for the heat generation case Q=35kW is shown for the whole model. The temperatures range from some 600K at the top of the cylindrical part to nearly 1500K in the upper third of the melt pool. **Figure 7** gives a more detailed view of the hemispherical part. For a clearer presentation the temperature scale ranges from 1160K to 1500K, the grey regions of the model have temperatures below 1160K.

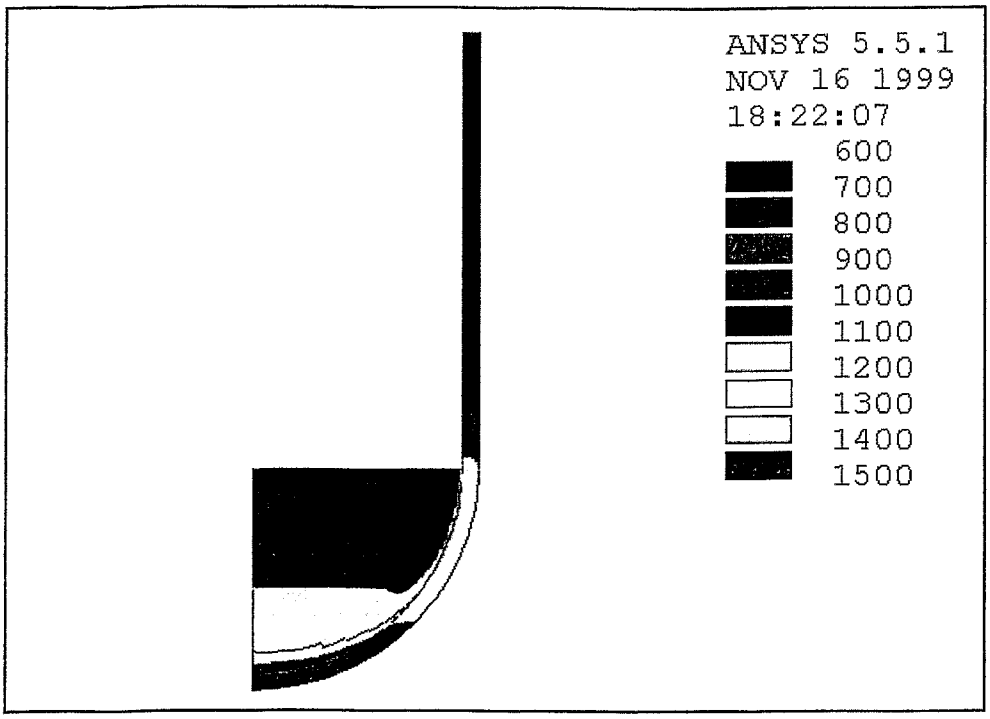

Figure 6: Calculated temperature field within whole computational domain after reaching quasi-stationary state with a power input of Q=35kW. T in [K]. Model figure is to scale and shown completely.

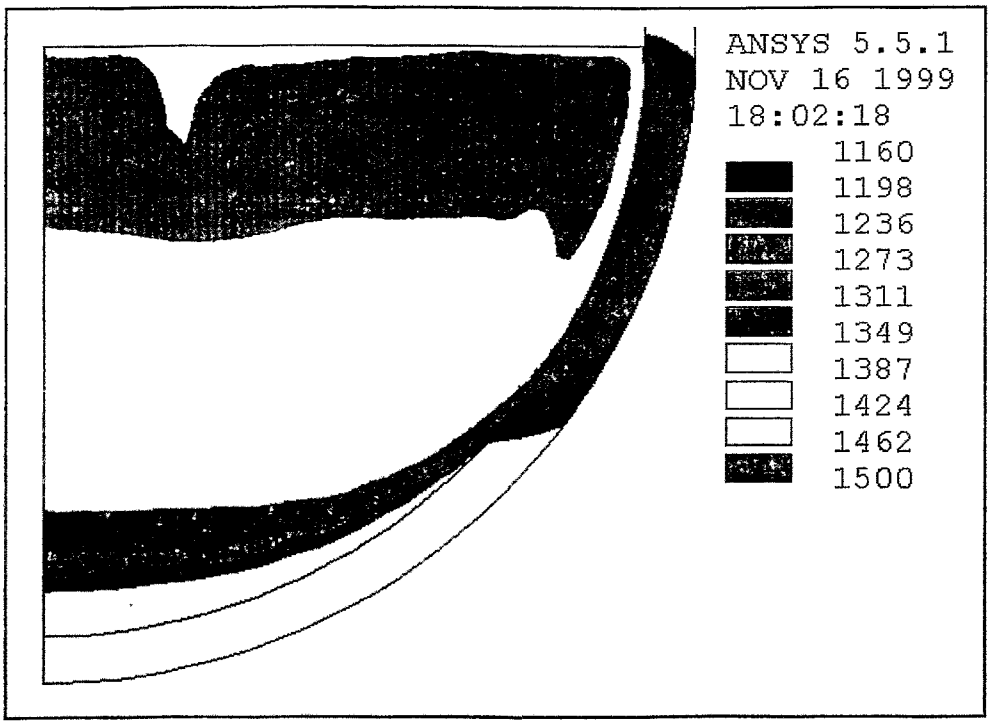

Figure 7: Calculated temperature field in the hemispherical part with a power input of Q=35kW. T in [K], adjusted scale ranges from 1160K to 1500K, temperatures below 1160K are presented grey.

The cooling effect at the vessel wall in the melt pool can be recognized easily, also the steep temperature gradient through the upper hemispherical part of the vessel wall caused by the focused heat transfer in this region. The melt shows a stable stratification in the lower and middle parts of the pool, while it has an unstable behaviour near the pool surface where cold plumes are to be found irregularly except close to the wall. The crust acts as an effective insulation and the vessel temperature drops down towards the bottom center. In **Figure 8** the external vessel surface temperature calculated for three different power inputs is compared with the measured temperatures at different times. The positions of the thermocouples (TC) are indicated with squares in the diagram. The connecting lines between the TCs should only give an orientation because the distances between the TCs are too large.

The calculated temperature profiles show good agreement with the measurements in the high temperature region of the vessel (cf. **Fig. 8**). For the slight offset between the temperature maxima it must be mentioned that the CFD-calculations assume the melt level exactly at the welding joint whereas in reality the melt level could have been 10mm to 20mm higher at the beginning. Later the melt level was decreasing due to the volume expansion of the creeping vessel. Also the vertical movement of the thermocouples (positions marked with squares in the curves) fixed to the side- and downwards creeping vessel wall is not taken into account in the figure.

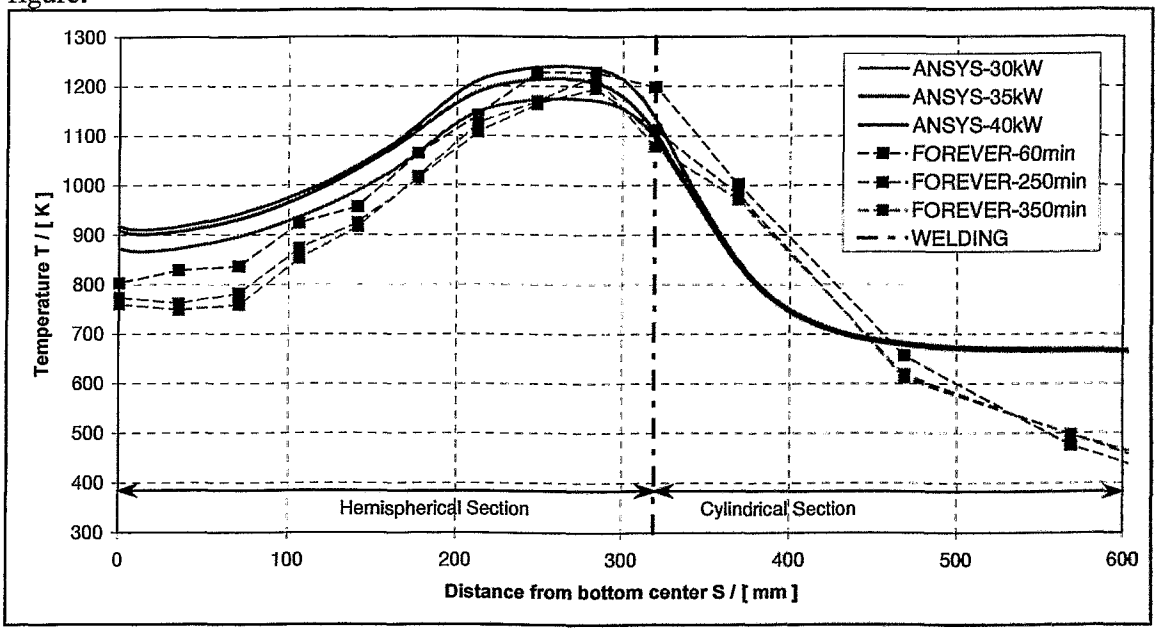

Figure 8: Comparison of external vessel surface temperature T / [K] at different times during the experiment and that calculated by ANSYS for different power inputs. Abscissa starts at very bottom centre and shows the chord length to the top of the cylinder.

The differences near the bottom center could result from the transient increase of the distance between the lowermost parts of the heater to the vessel bottom, which is not modelled so far. Another possibility is the formation of a gap between oxidic crust and vessel wall, which induces additional heat transfer resistance. The examination of the vessel after the experiment could not clearly exclude that there was a gap at the vessel bottom before heater failure. However, no gap was observed in the examination after the experiment, and no gap is modelled in the computations. Later, it will be seen that the combination of low temperatures and low

stresses in this region causes no creep near the bottom centre. Also, the temperatures in the upper part of the cylinder are too low to cause significant damage. Therefore the differences between the calculated values and measurements are acceptable. In future more detailed boundary conditions for the cylinder should improve the results.

Corresponding to the external thermocouples internal thermocouples were installed but they all failed just 15 min after melt arrival in the vessel. The reason for the failure is not exactly known, it can be due to fast thermal expansion of the vessel at the beginning which caused the ripping of the exactly fitted TC-wires or the aggressive melt dissoluted the thermocouples or their connection to the wires. Therefore no comparison between the experimental and the calculated temperatures for the vessel inside is possible.

Figure 9 shows the calculated temperature profiles on the vessel inside for different power input scenarios in comparison to the calculated external surface temperature. The resulting temperature difference over the wall thickness is according to the local heat flux through the wall for each power scenario. So far, no transient CFD-calculation for the whole creep deformation stage has been performed due to the large computational time and data storage requirements. But a full time CFD-calculation for the whole creep deformation stage with detailed time-dependent power input is under preparation and with improved computational resources its results will be available in future.

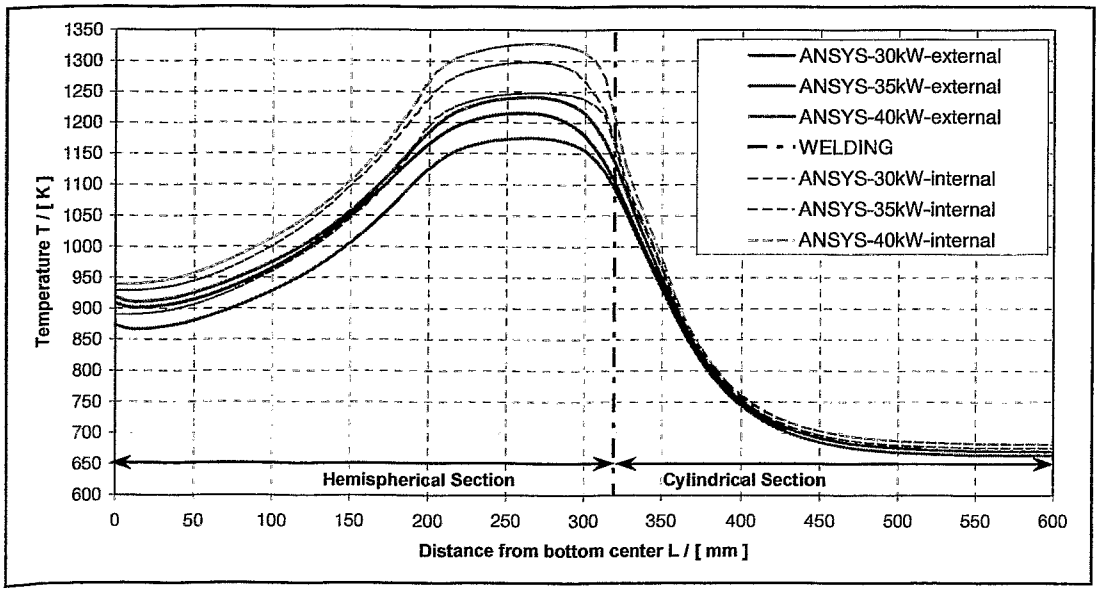

Figure 9: Calculated internal and external vessel wall temperature T / [K] for different power inputs. Abscissa starts at very bottom centre and shows the chord length to the top of the cylinder.

4 Advanced Creep Modelling

In the following sections the model for the structure- mechanical calculations is described. Because of the large spatial and transient temperature and stress changes within the vessel wall a new approach for the numerical creep modelling has been developed.

The creep behaviour of materials is usually described by analytical formulas (creep laws) with a number of free parameters, e.g. the creep strain rate is calculated by:

$$\dot{\varepsilon} = c_1 \cdot \sigma^{c_2} \cdot t^{c_3} \cdot \exp\left[-\frac{c_4}{T}\right] \qquad (4)$$

The coefficients (c_1... c_4 in eq. 4) are obtained by fitting the creep law to creep tests performed at constant load and temperature. However, in practice it is often difficult to achieve a satisfying adjustment for a wide range of temperatures and stresses with only one set of parameters. Instead, it appears that the parameters themselves are functions of the temperature or the stress level. Therefore a supplementary method is developed which allows to describe the creep behaviour of a material for different stress and temperature levels independently. This is especially useful if strong stress and/or temperature gradients are present. Additionally it is possible to calculate the creep damage and deactivate elements whose accumulated damage is greater or equal to one.
The user programmable features (UPF) of ANSYS® allow the user to couple his own routines to the standard FE-code.The Digital® Fortran Compiler (Rev. 6.0A) was used for programming and for generating the customized ANSYS-executable on a Windows/NT® platform.
The creep behaviour of a material can be described by the strain hardening representation:

$$\dot{\varepsilon}^{cr} = f(\varepsilon^{cr}; \sigma; T) \qquad (5)$$

The time hardening representation, or the work hardening representation, can, in general, be transformed into eq (5). The relation eq (5) is transferred into the ANSYS database by means of a number of discrete pairs of the form

$$\begin{bmatrix} \varepsilon_{(1)} & \dot{\varepsilon}_{(1)} \\ \vdots & \vdots \\ \varepsilon_{(n)} & \dot{\varepsilon}_{(n)} \end{bmatrix}_{T=\text{const};\sigma=\text{const}} \qquad (6)$$

Several of such sets for different temperature and stress levels can be combined. The complete creep data base then is shown in table 1.

T_1			⋯	T_K		
$\sigma_{1;1}$	⋯	$\sigma_{1;M1}$	⋯	$\sigma_{K;1}$	⋯	$\sigma_{K;MK}$
$\varepsilon^{frac}_{1;1}$	⋯	$\varepsilon^{frac}_{1;M1}$	⋯	$\varepsilon^{frac}_{K;1}$	⋯	$\varepsilon^{frac}_{K;MK}$
$N_{1;1}$	⋯	N_{M1}	⋯	$N_{K;1}$	⋯	$N_{K;MK}$
$(\varepsilon_{1;1;1};\dot{\varepsilon}_{1;1;1})$	⋯	$(\varepsilon_{1;M1;1};\dot{\varepsilon}_{1;M1;1})$	⋯	$(\varepsilon_{K;1;1};\dot{\varepsilon}_{K;1;1})$	⋯	$(\varepsilon_{K;MK;1};\dot{\varepsilon}_{K;MK;1})$
⋮	⋱	⋮	⋱	⋮	⋱	⋮
$(\varepsilon_{1;1;N};\dot{\varepsilon}_{1;1;N})$	⋯	$(\varepsilon_{1;M1;N};\dot{\varepsilon}_{1;M1;N})$	⋯	$(\varepsilon_{K;1;N};\dot{\varepsilon}_{K;1;N})$	⋯	$(\varepsilon_{K;MK;N};\dot{\varepsilon}_{K;MK;N})$

Table 1: Principle configuration of a creep database for a temperature range from T_1 to T_K and a stress range from σ_1 to σ_M including the respective creep rupture strain ε^{frac}.

The first index refers to the temperature, the second index to the stress and the third to the strain. K is the number of temperature levels, Mk the number of stress levels within the k-th temperature level and $N_{k;m}$ the number of strain rate-strain pairs for the m-th stress level within the k-th temperature level.
The UPF routine user01 (ANSYS, 1998) is used to realize the creep data input into ANSYS. The data must be provided by the user as a set of ASCII files (for each temperature-stress level one file). To realize the calculation of the creep strain increment according to the non-standard creep law, the UPF usercr.f was modified and linked to the customized ANSYS executable (ANSYS, 1998).

In this routine the scalar creep strain increment $\Delta\varepsilon^{cr} = \dot{\varepsilon}^{cr} \cdot \Delta t$ is determined from the creep data (cf. Table 1) by multi-linear interpolation:

$$\begin{aligned}\Delta\varepsilon^{cr} = [&w_1 \cdot \dot{\varepsilon}_{L;L;L} + w_2 \cdot \dot{\varepsilon}_{L;L;H} + w_3 \cdot \dot{\varepsilon}_{L;H;L} + w_4 \cdot \dot{\varepsilon}_{L;H;H} \\ &+ w_5 \cdot \dot{\varepsilon}_{H;L;L} + w_6 \cdot \dot{\varepsilon}_{H;L;H} + w_7 \cdot \dot{\varepsilon}_{H;H;L} + w_8 \cdot \dot{\varepsilon}_{H;H;H}] \cdot \Delta t\end{aligned} \qquad (7)$$

with w_i being the weighting factors (eq. 8):

$$
\begin{aligned}
w_1 &= \frac{(T_H - T)\cdot(\sigma_{L;H} - \sigma)\cdot(\varepsilon_{L;L;H} - \varepsilon)}{(T_H - T_L)\cdot(\sigma_{L;H} - \sigma_{L;L})\cdot(\varepsilon_{L;L;H} - \varepsilon_{L;L;L})} \\
w_2 &= \frac{(T_H - T)\cdot(\sigma_{L;H} - \sigma)\cdot(\varepsilon - \varepsilon_{L;L;L})}{(T_H - T_L)\cdot(\sigma_{L;H} - \sigma_{L;L})\cdot(\varepsilon_{L;L;H} - \varepsilon_{L;L;L})} \\
w_3 &= \frac{(T_H - T)\cdot(\sigma - \sigma_{L;L})\cdot(\varepsilon_{L;H;H} - \varepsilon)}{(T_H - T_L)\cdot(\sigma_{L;H} - \sigma_{L;L})\cdot(\varepsilon_{L;H;H} - \varepsilon_{L;H;L})} \\
w_4 &= \frac{(T_H - T)\cdot(\sigma - \sigma_{L;L})\cdot(\varepsilon - \varepsilon_{L;H;L})}{(T_H - T_L)\cdot(\sigma_{L;H} - \sigma_{L;L})\cdot(\varepsilon_{L;H;H} - \varepsilon_{L;H;L})} \\
w_5 &= \frac{(T - T_L)\cdot(\sigma_{H;H} - \sigma)\cdot(\varepsilon_{H;L;H} - \varepsilon)}{(T_H - T_L)\cdot(\sigma_{H;H} - \sigma_{H;L})\cdot(\varepsilon_{H;L;H} - \varepsilon_{H;L;L})} \\
w_6 &= \frac{(T - T_L)\cdot(\sigma_{H;H} - \sigma)\cdot(\varepsilon - \varepsilon_{H;L;L})}{(T_H - T_L)\cdot(\sigma_{H;H} - \sigma_{H;L})\cdot(\varepsilon_{H;L;H} - \varepsilon_{H;L;L})} \\
w_7 &= \frac{(T - T_L)\cdot(\sigma - \sigma_{H;L})\cdot(\varepsilon_{H;H;H} - \varepsilon)}{(T_H - T_L)\cdot(\sigma_{H;H} - \sigma_{H;L})\cdot(\varepsilon_{H;H;H} - \varepsilon_{H;H;L})} \\
w_8 &= \frac{(T - T_L)\cdot(\sigma - \sigma_{H;L})\cdot(\varepsilon - \varepsilon_{H;H;L})}{(T_H - T_L)\cdot(\sigma_{H;H} - \sigma_{H;L})\cdot(\varepsilon_{H;H;H} - \varepsilon_{H;H;L})} \\
&\left(\sum_{i=1}^{8} w_i = 1\right)
\end{aligned}
\qquad (8)
$$

The quantities without index ε, σ, T are the actual values of the current element integration point. The indexed quantities are the values from the creep data base eq. (3). They form the smallest intervals which the actual quantities are enclosed in. The meaning of the indices is L: low bound (largest data base value which is smaller than the actual integration point value) and H: high bound (smallest data base value which is greater than the actual integration point value). The first index refers to the temperature, the second index to the stress and the third to the strain. All stress and strain values used here are equivalent values. The components of the creep strain tensor increment, $\Delta\varepsilon_{kl}^{cr}$, are calculated according to the Prandtl-Reuss flow rule (ANSYS, 1998, Becker, 1995).

The creep data base (cf. Table 1) has to be provided in such a way that the actual temperature and the equivalent stress of the elements do not exceed the maximum values of the creep data base. If the actual temperature or stress values are smaller than the smallest values provided, the creep strain increment is zero for this step.

The material damage due to significant creep strains is modelled by a damage measure which is incrementally accumulated at the end of a load step. The damage increment is:

$$\Delta D = \frac{\Delta \varepsilon_{eqv}^{cr}}{\varepsilon_{frac}^{cr}(\sigma, T)} \cdot \frac{\sigma_{eqv}}{\left|\sigma_1 + \sigma_2 + \sigma_3\right|} \qquad (9)$$

with ε_{frac}^{cr} being the creep fracture strain of the uniaxial creep test at constant stress and temperature. The factor $\sigma_{eqv} / \left|\sigma_1 + \sigma_2 + \sigma_3\right|$ (where σ_{eqv} is the von-Mises equivalent stress) considers the damage behaviour in dependance on the tri-axiality of the stress tensor (Azodi et al., 1996). The damage increment is calculated for each finite element by averaging its nodal equivalent creep strains. The accumulated damage over all load steps is

$$D = \sum_{i=1}^{ldstep} \Delta D_i \qquad (10)$$

If the element damage reaches the value of D=1, the element is killed by setting its death flag to 1 (refer to the „element birth and death" section of ANSYS 1998).
The creep fracture strain used for the evaluation of the damage increment can be calculated according to a temperature and stress dependent function with user supplied constants or it is calculated from the creep data base (cf. Table 1) by multi-linear interpolation.

5 Description of the Mechanical Model

The mechanical 2D-axis-symmetric model representation which approximates the 3D-vessel consists of nearly 340 elements and some 410 nodes with 5 element layers over the wall thickness. A sufficient number of elements over the wall thickness is necessary to model the transient body load of the temperature field which is changing along and perpendicular to the wall surface. This is seen in **Figure 10**, which shows the temperature field caused by the 30kW-scenario as body load of the mechanical model.

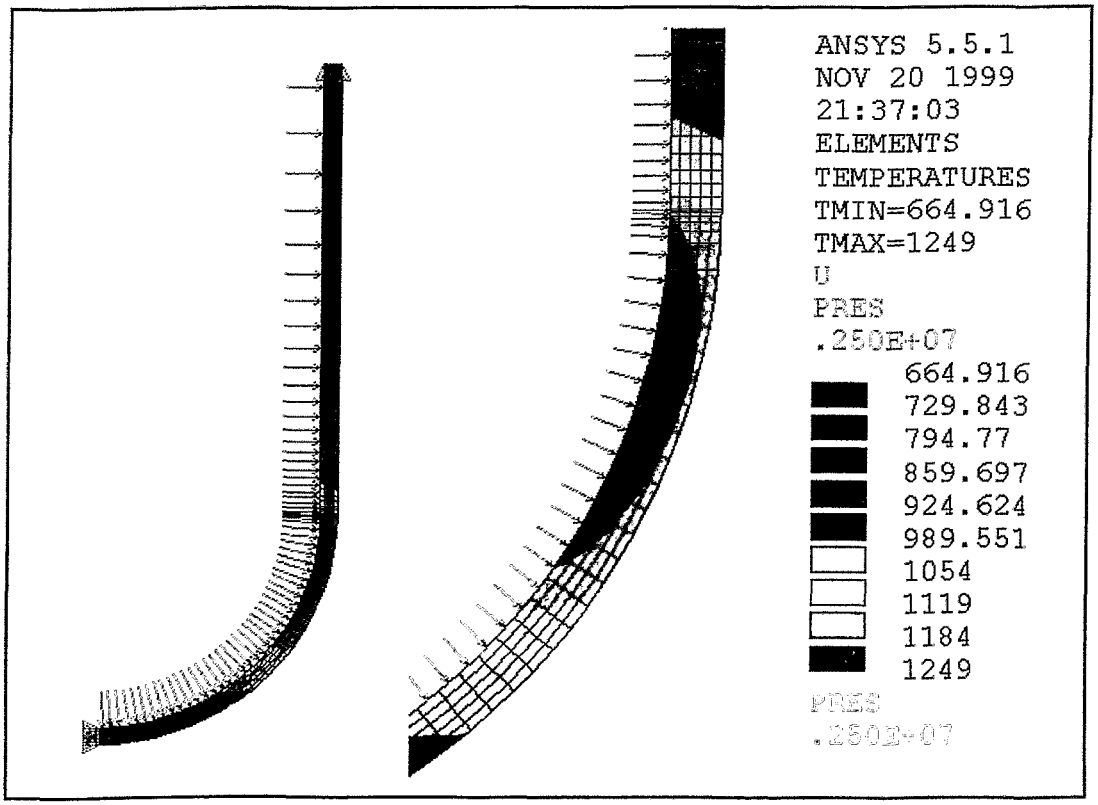

Figure 10: Mechanical FE-model with applied boundary conditions, surface loads and body loads: U_y=0 at top, U_x=0 at symmetry line, internal pressure P=2.5MPa, temperature field caused by power input Q=30kW. Left side total view, right side detail of hot focus region.

Figure 10 also shows the internal pressure load of P=2.5MPa and the boundary conditions of zero vertical displacement (U_y=0) at the vertical top end and zero radial displacement (U_x=0) at the symmetry axis.

For the mechanical calculations isotropic material behaviour is assumed. The temperature dependence of all material properties is considered according to the known values of the French 16MND5 RPV steel (Sehgal et al., 1999). The creep data base (cf. Table 1) has been generated from the fitted strain curves developed by Ikonen (1999). The stress range of the data base reaches from σ_{min} = 5MPa to σ_{max} = 285MPa and the temperature range goes from T_{min}=873K to T_{max}=1373K. That means the calculation is finished if the corresponding maximum values are exceeded.

6 Post Test Creep Calculations

Until pressurization of the system the displacement measured by the linear displacement transducers (LDT) is only due to thermal expansion. Therefore the transient creep calculation starts at the pressurization time of t=12000s (cf. **Figs. 3** and **11**), in the experiment. If a constant temperature field is assumed within the vessel wall for the transient creep calculation a typical creep curve will be calculated by the code (see **Fig. 11**, blue curve). This curve is characterized by a steep - but decreasing - rate of creep strain. This is the so called primary creep stage. After that the creep strain rate becomes nearly constant, this stage is known as secondary creep. If the creep process is not stopped there will be a third stage - the tertiary creep - which shows the opposite behaviour of primary creep and is immediately followed by the rupture of the structure.

In fact the total displacement in the experiment (black curve) shows a quite different behaviour. The curve looks like a tertiary creep curve, but considering the stress and temperature regimes at this time and the total duration of 3 hours tertiary creep is very unlikely.

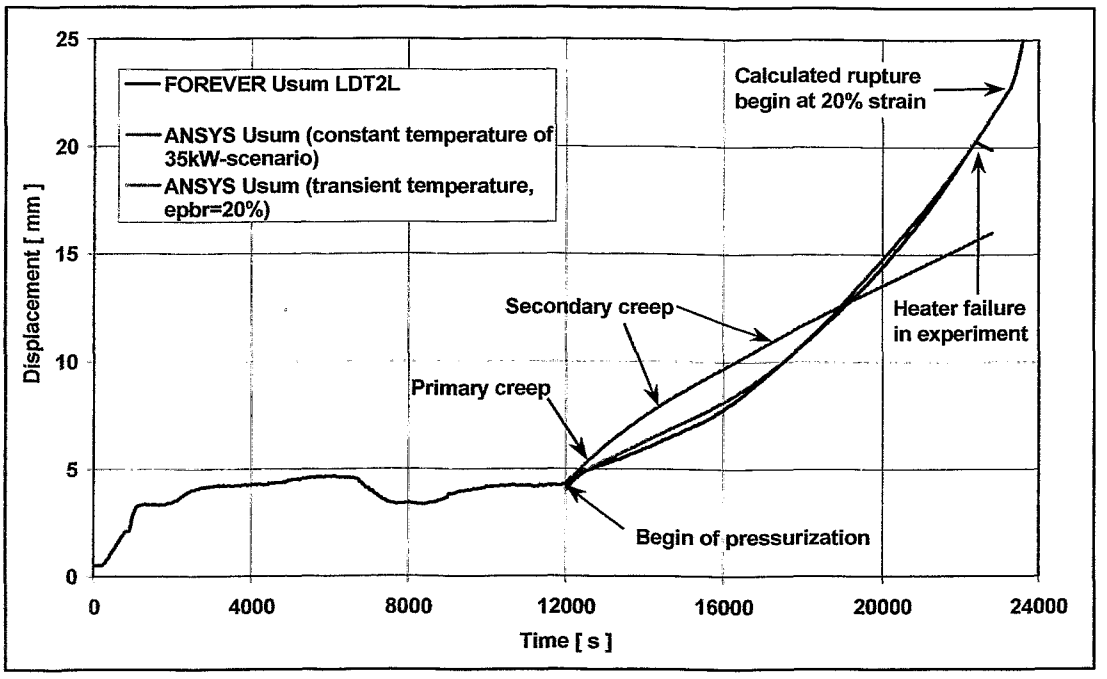

Figure 11: Total displacement U_{sum} / [m] of the vessel external surface on the left side at position $\Theta = 134°$ over time t / [s].

Performing a transient calculation with a changing temperature field according to the recorded power input (cf. **Fig. 2**) the calculated creep follows the red curve in **Fig. 11**. For this calculation the steady state temperature fields of the CFD-calculations with 30, 35 and 40kW were considered and a time delay of 15min between the power change and the change of the temperature field was assumed. Consequently the temperature at the beginning of the creep deformation stage is decreasing due to a power decrease just before pressurization (cf. **Fig. 2** and **3**). From this relatively low level the temperature increases after the first half hour of creep until heater failure. Within these steps the temperature is linearly interpolated. Of course this model has to be improved and as mentioned before this will be possible with a transient temperature field available from the CFD-result file.

Figure 12 shows the calculated horizontal and vertical displacement of the vessel at the time of heater failure (t=22,800s). The maximum value for the radial displacement is to be found in the hot focus region (ca. 14mm) while the maximum vertical displacement (ca. -21mm) can be seen between θ=120° and θ=150° (θ=180° refers to the very bottom). For a comparison the total displacement and the Von Mises equivalent stress at this time are shown in **Figure 13.** The maximum total displacement of nearly 23mm is according to the combination of the radial and vertical displacement. On the other hand the maximum equivalent stress of some 180 MPa is not to be found in regions of large displacements or high temperatures (cf. **Fig. 10**). In the following we will also have a look on the stress components and the according strains.

Figures 14 and **15** show the different stress components and the resulting Von Mises equivalent stress, which is printed again for convenience. It can be seen that the vertical and circumferential stresses give the main contribution to the maximum equivalent stress above the hot focus region. These high stresses seem to result from the outwards deformation of the upper part of the hemisphere, which causes a bending moment in the cylindrical part above.

Due to the higher temperatures in the hot focus region smaller stresses can cause larger strains than observed in the regions with the highest stresses but lower temperatures. Horizontal and vertical strain are displayed in **Figure 16.** It should be noted that the wall thinning and stretching in the hot focus region is clearly visible: radially the wall is thinned by 20% (negative scale values) and vertically it is stretched by nearly 15%. In **Figure 17** the circumferential and the equivalent strain are represented. As it could be expected the highest values belong to the hot focus region.

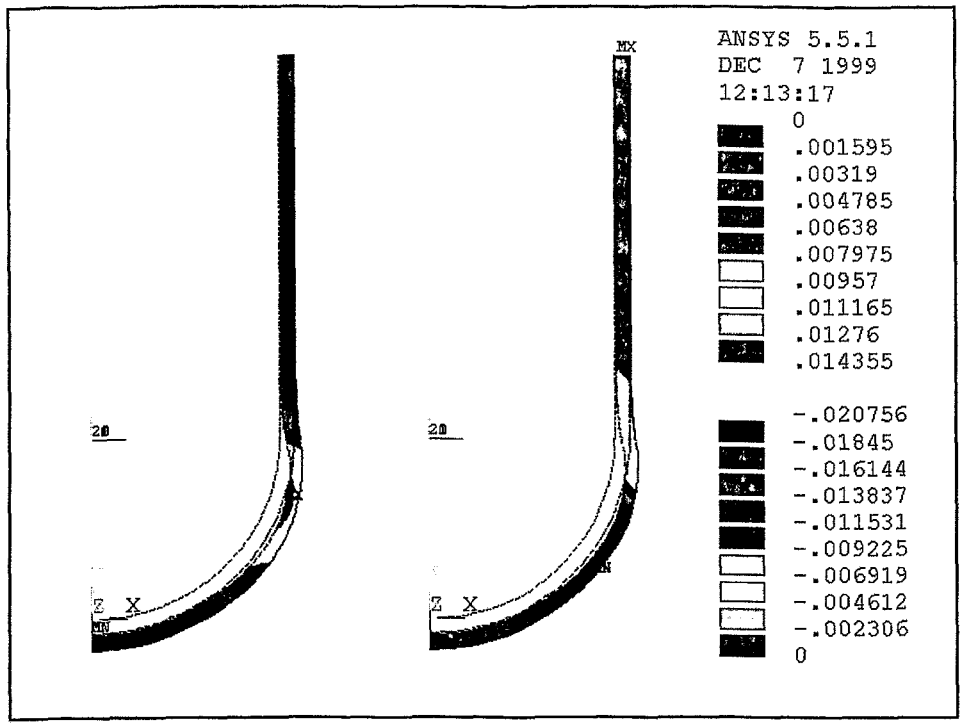

Figure 12: Horizontal displacement U_x / [m] (left side and upper scale) and vertical displacement U_y / [m] (right side and lower scale) after t=22,800s (heater failure).

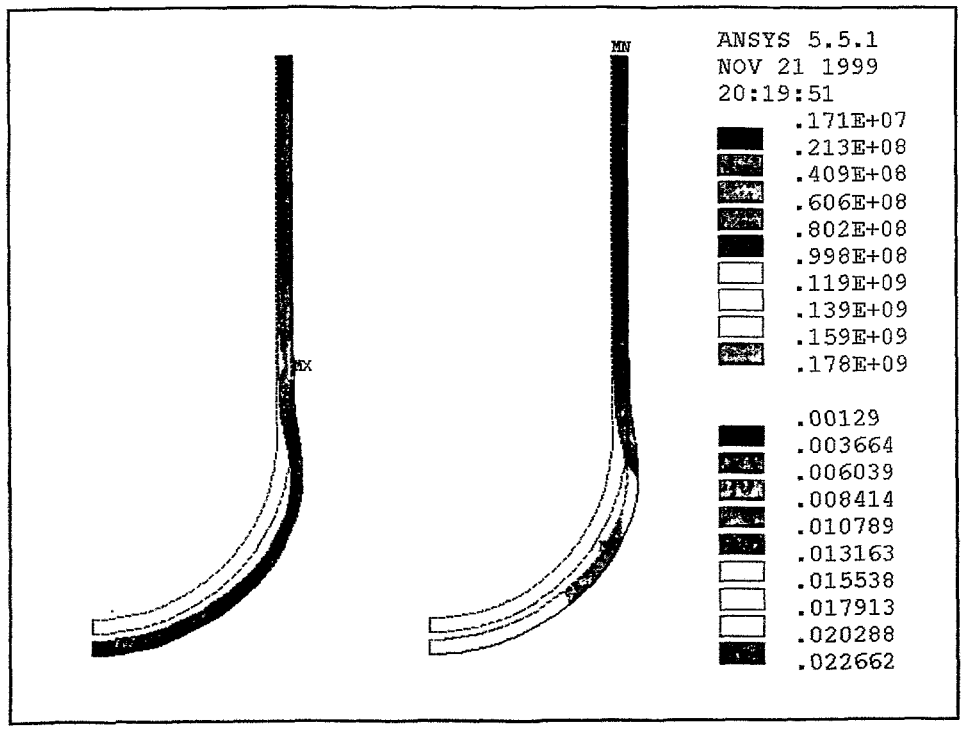

Figure 13: Von Mises equivalent stress σ_{eqv} / [Pa] (left side and upper scale) and total displacement U_{sum} / [m] (right side and lower scale) of the vessel after t=22,800s (heater failure).

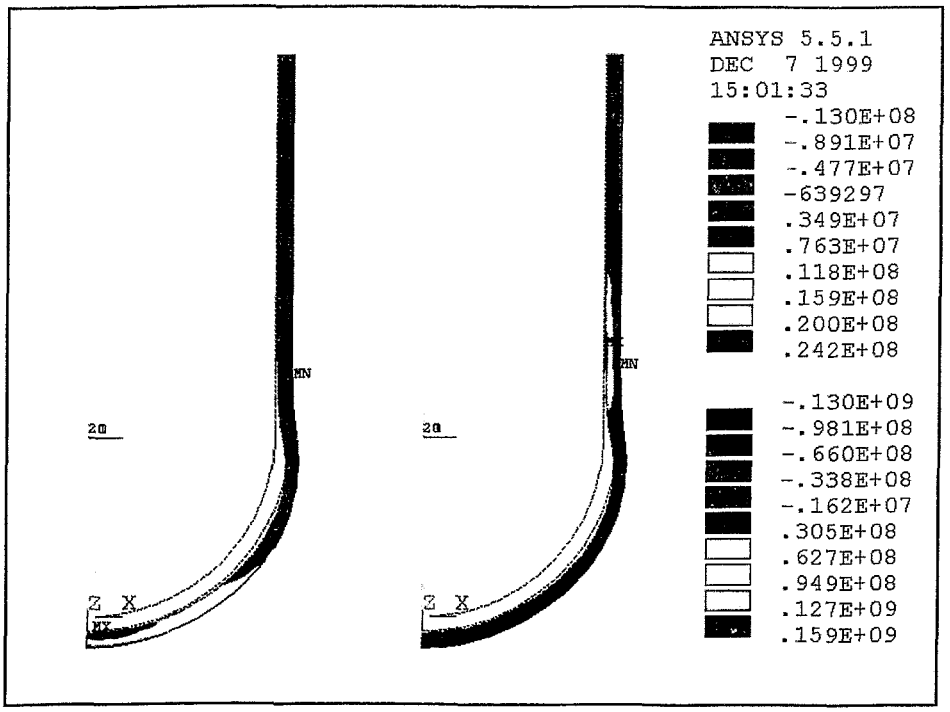

Figure 14: Horizontal stress σ_x / [Pa] (left side - upper scale) and vertical stress component σ_y / [Pa] (right side - lower scale) after t=22,800s (heater failure).

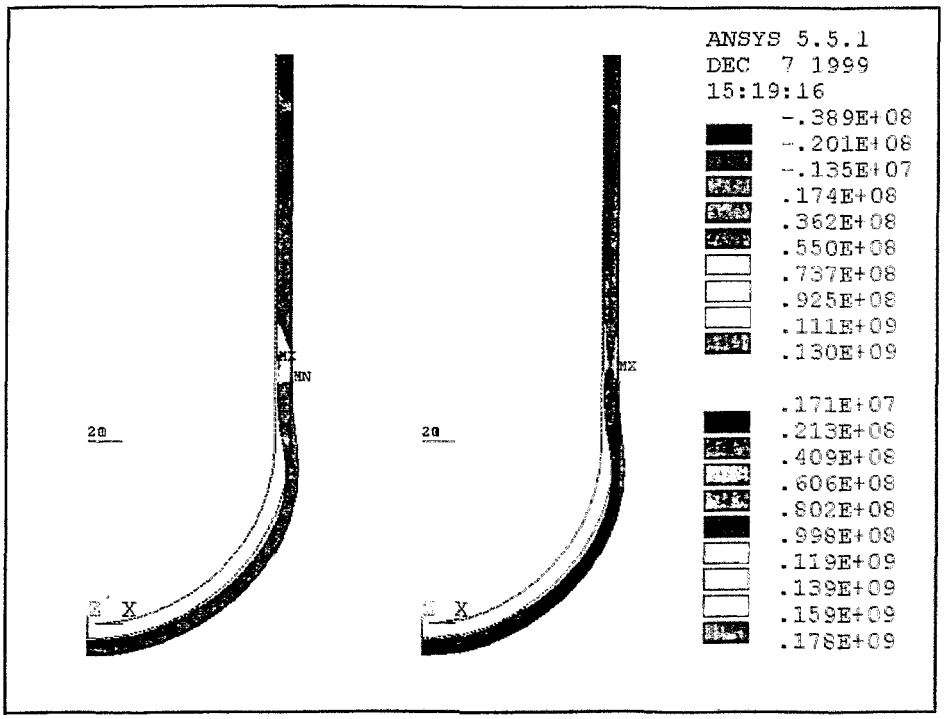

Figure 15: Circumferential stress component σ_c / [Pa] (left side - upper scale) and equivalent stress σ_{eqv} / [Pa] (right side - lower scale) after t=22,800s (heater failure).

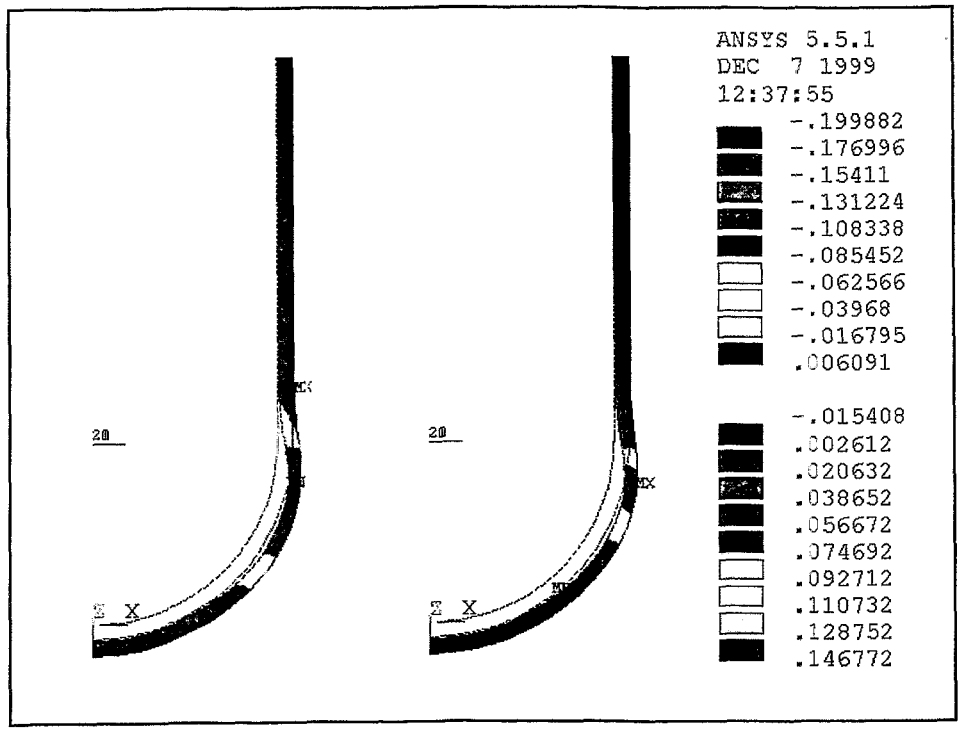

Figure 16: Horizontal strain ε_x / [-] (left side - upper scale) and vertical strain ε_y / [-] (right side - lower scale) after t=22,800s (heater failure).

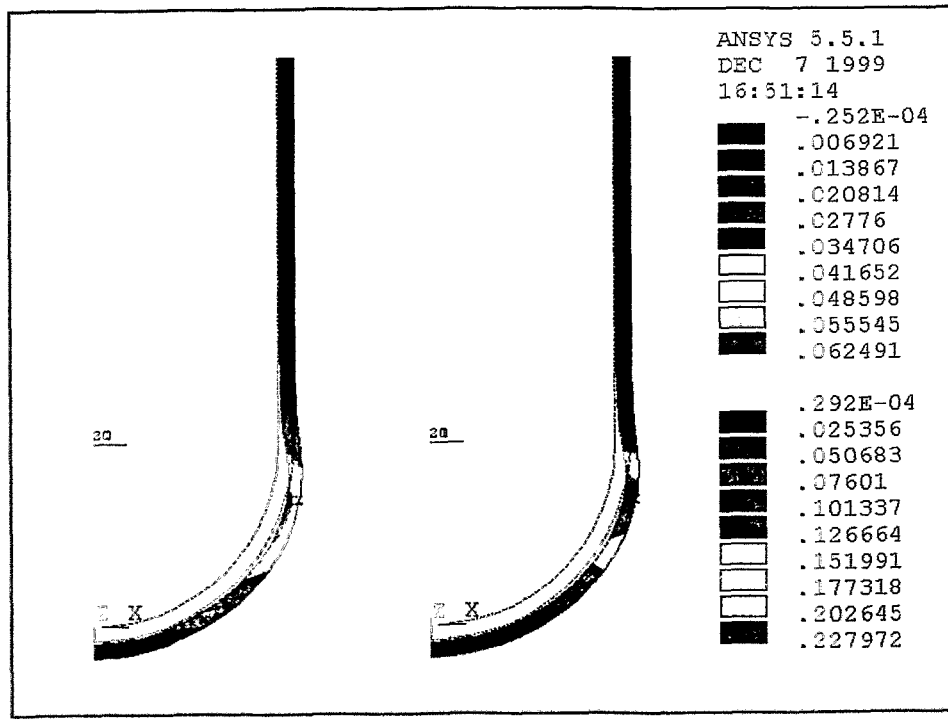

Figure 17: Circumferential strain ε_c / [-] (left side - upper scale) and total strain ε_{sum} / [-] (right side - lower scale) after t=22,800s (heater failure).

As mentioned the heater failure occurred due to the uncovering of the top ends of the heater rods. A volume calculation of the deformed vessel shows that the melt level at this time had dropped by 33mm, assuming a total height of the melt of 188mm at the beginning, which is equivalent to the inner radius of the hemisphere.

Comparing **Figures 18** and **19** it can be seen that not at all positions the calculation fits with the experimental data. The discrepancies are greater in the upper part of the hemisphere and at the beginning of the cylindrical part. This could be due to the vertical offset of the calculated temperature field and the measured one. The effect of the offset is eliminated in the lower parts ($134° < \Theta < 180°$) where the calculation is in good agreement with the experiment.
In the diagrams the calculated curves run until vessel failure, while the experimental curves run until heater failure. For this calculation an uniform fracture strain of 20% was assumed, which is very conservative and will be discussed in the next chapter. But it should be noted that the vertical displacement is reverse between the case of reaching heater failure and reaching vessel failure.

Another possibility to check the accordance of the calculation with the experimental results is shown in the **Figures 20, 21** and **22.** The local distribution of the vessel wall thickness has been recorded before (ultrasonic measurement) and after the experiment (calliper rule). Due to the 2D-FE-model these values have to be averaged at the different elevations before the subtraction. **Figure 22** shows the experimental results as black crosses. The red line shows the wall thickness change evaluated by the FE-calculation. Again the wall thinning in the hot focus region is clearly visible and agrees very well with the experimental results. The positive measured values at the bottom centre may result from the different measurement techniques. For the FE-results the explanation is the thermal expansion, which has not been subtracted from the final wall thickness.

For a first summary it can be stated that the Finite-Element-Model is able to describe the main processes and phenomena for creep stages until those reached in FOREVER-C2. In the next chapter the possible further development until failure is discussed.

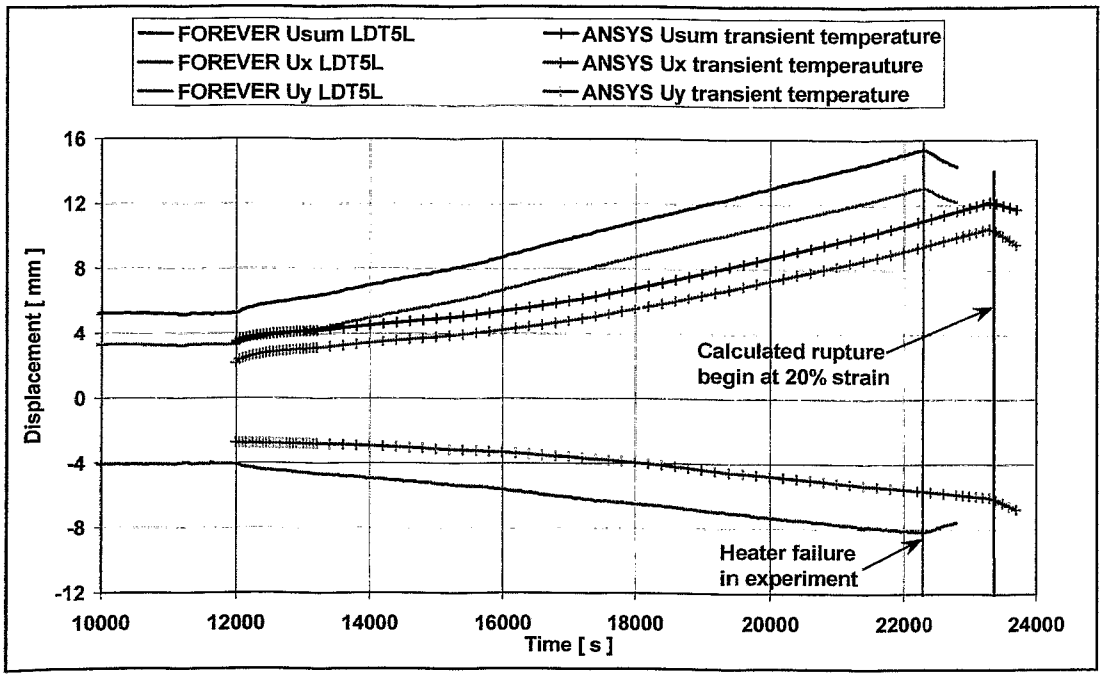

Figure 18: Total displacement U_{sum} / [m], horizontal displacement U_x / [m] and vertical displacement U_y / [m] of the vessel external surface on the left side at position $\Theta = 96°$ over time t / [s].

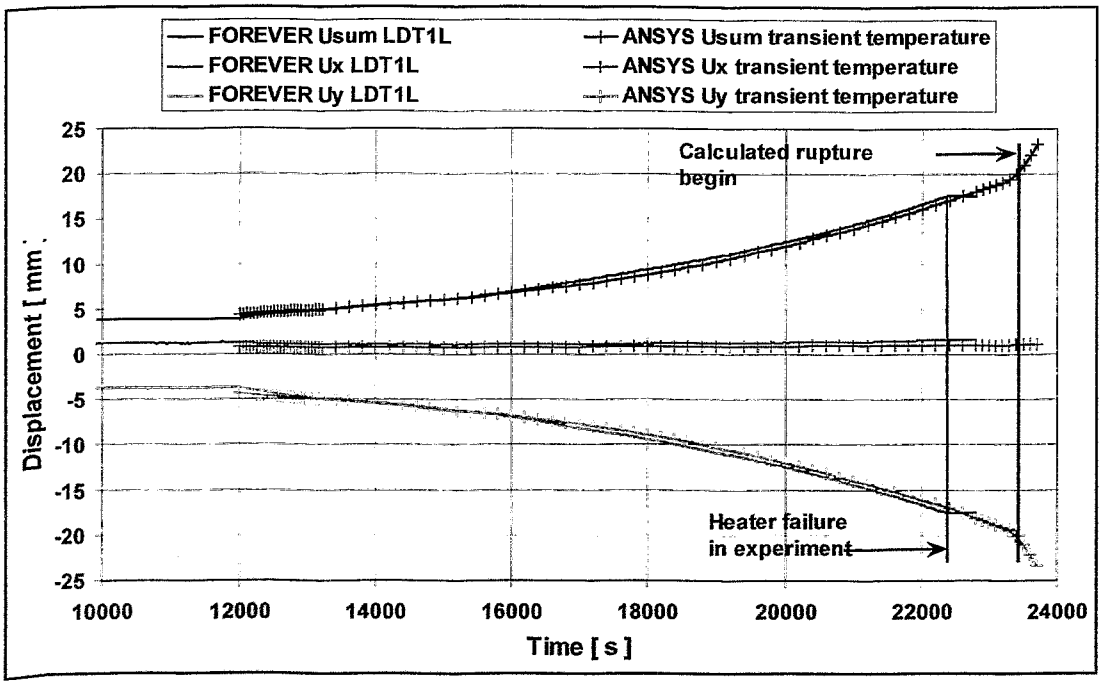

Figure 19: Total displacement U_{sum} / [mm], horizontal displacement Ux / [mm] and vertical displacement Uy / [mm] of the vessel external surface on the left side at position $\Theta = 154°$ over time t / [s].

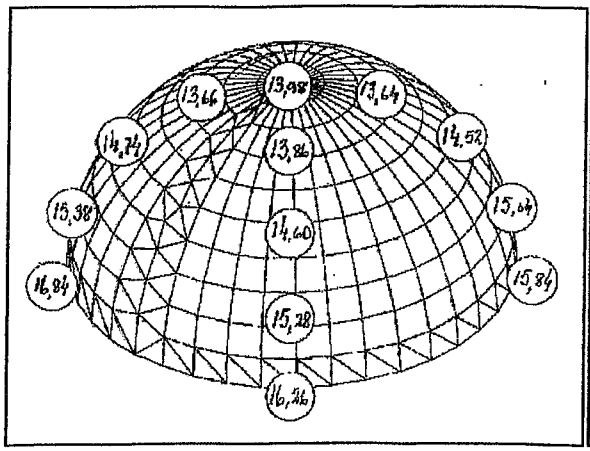

Figure 20: Measured wall thickness s_b / [mm] before experiment.

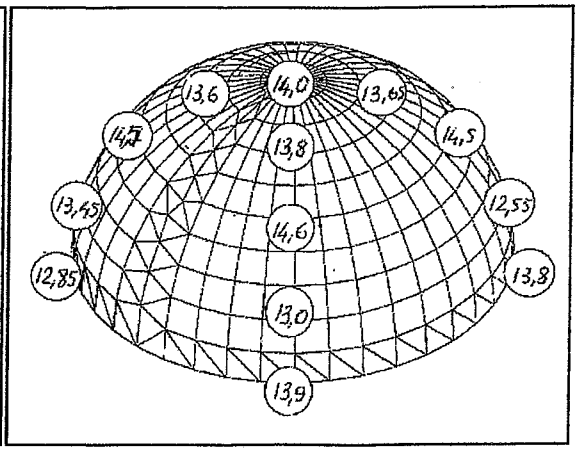

Figure 21: Measured wall thickness s_a / [mm] after experiment.

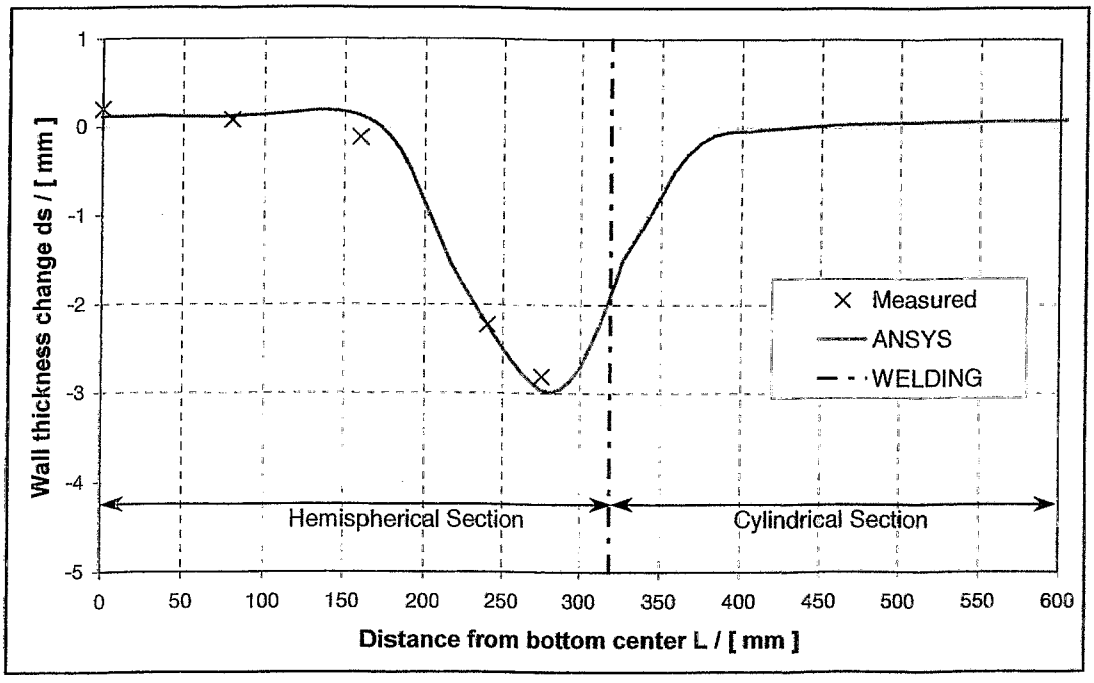

Figure 22: Wall thickness change $ds=s_a-s_b$ / [mm] defined as difference of the wall thickness after s_a and before s_b the experiment plotted over the vessel shape.

7 First Estimation of Failure Time

The most interesting question for the next experiments is the vessel failure time. It is not intended to have the vessel fail at the high pressure load. Therefore, different scenarios have to be calculated. In the calculations shown here the temperature increase after the unintentional heater failure in FOREVER-C2 has been set to 10K/h and the high pressure load was kept on until vessel failure. So these calculations could also be called „No-Heater-Failure"-calculations. With an assumed very conservative creep rupture strain of ε^{frac}=20% for all stresses and temperatures for the evaluation of the damage parameter D, this leads to a vessel failure at t_{frac}=23,700s (cf. **Figs. 18, 19** and **23**). This means just 15min after the heater failure in FOREVER-C2 the vessel would have failed. But considering the uniaxial creep test data of the 16MND5-steel (Ikonen, 1999) and the results of the Lower Head Failure Tests (Chu et al., 1999) at the Sandia National Laboratories even a creep rupture strain of ε^{frac}=40% can be stated as conservative. **Figure 23** shows the total displacement at Θ=134° for both cases. In the 40%-scenario failure could be expected after t_{frac}=28800s, which means more than one hour after heater failure in FOREVER-C2. In the tests mentioned before also fracture strains of more than 60% were observed. Assuming a fracture strain of 60% vessel failure would occur after 525 min (i.e. 345 min after pressurization).

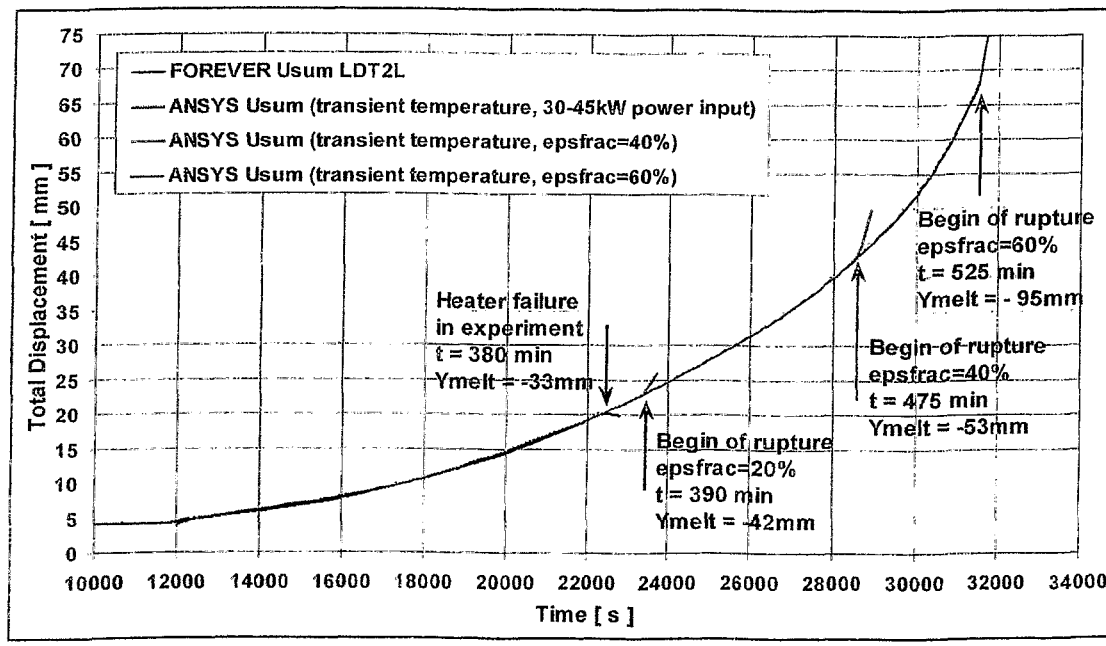

Figure 23: Estimation of vessel failure time with different creep rupture strains. Total displacement U_{sum} / [mm] of the vessel external surface on the left side at position Θ = 134° over time t / [s].

The **Figures 24, 25** and **26** show the total displacement and the equivalent strains for the different scenarios (cf. **Fig. 23**). It should be noted that the maximum strain can be higher than the assumed maximum fracture strain due to the tri-axiality factor in equation (9). This factor can be smaller than one if a full or partial hydrostatic stress regime exist. Then the final strain can be larger than the assumed creep fracture strain for the uniaxial case. Due to the larger expansion of the vessel under the assumption of larger fracture strains the melt level drop is increased. For the 40%-fracture strain scenario it would be y_{melt}= -53mm instead of -33mm at the

time of heater failure. And for the 60%-fracture-strain scenario a melt drop of 95mm is calculated. **Figure 27** shows a contour plot of the damage parameter in the 40%-fracture-strain scenario just before the first element reaches a value of 1 and is killed (t=28,300s), which initiates vessel failure. Of course, this is a first estimate and additional analysis will be performed when vessel failure is achieved in the experiments to come.

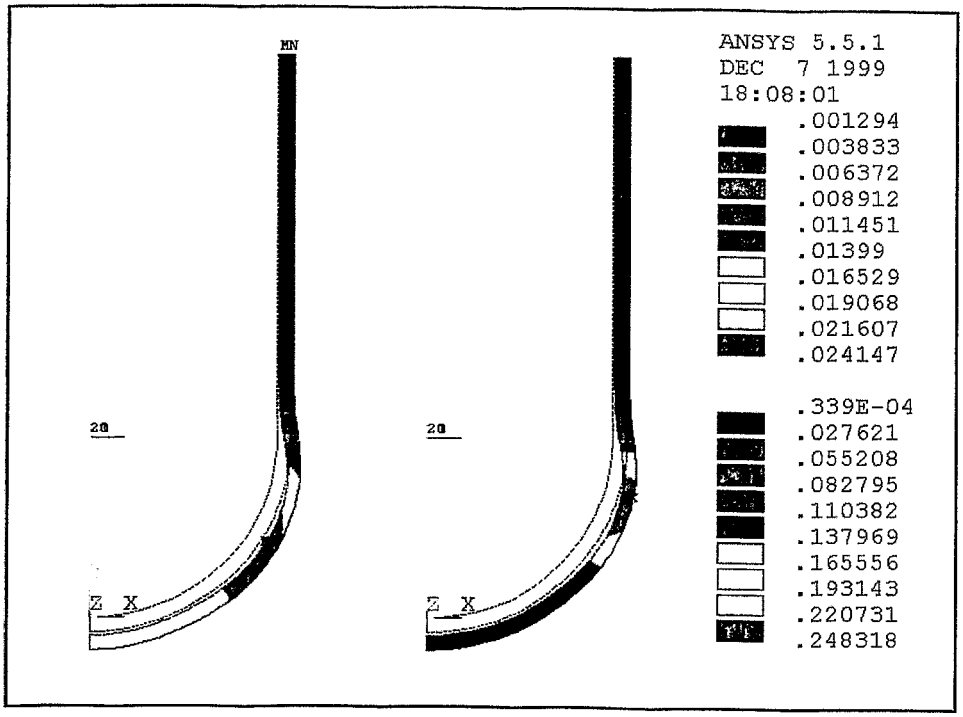

Figure 24: Total displacement U_{sum} / [m] (left side and upper scale) and Von Mises equivalent strain ε_{eqv} / [-] (right side and lower scale) of the vessel at t = 390min, assumed fracture strain ε_{frac}=20%.

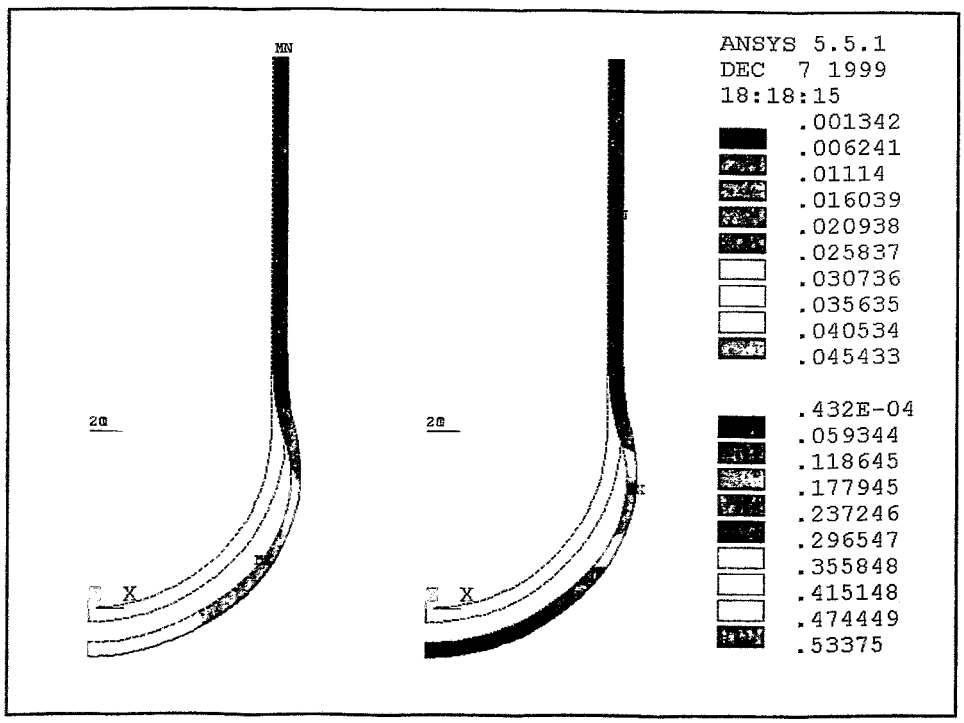

Figure 25: Total displacement U_{sum} / [m] (left side and upper scale) and Von Mises equivalent strain ε_{eqv} / [-] (right side and lower scale) of the vessel at t = 475min, assumed fracture strain ε_{frac}=40%.

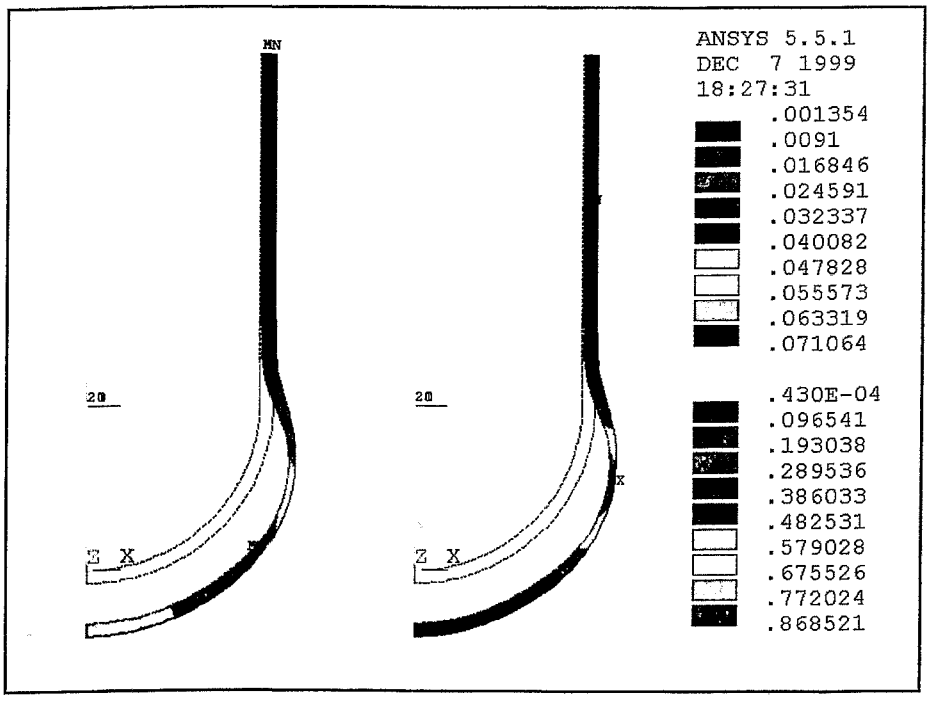

Figure 26: Total displacement U_{sum} / [m] (left side and upper scale) and Von Mises equivalent strain ε_{eqv} / [-] (right side and lower scale) of the vessel at t = 525min, assumed fracture strain ε_{frac}=60%.

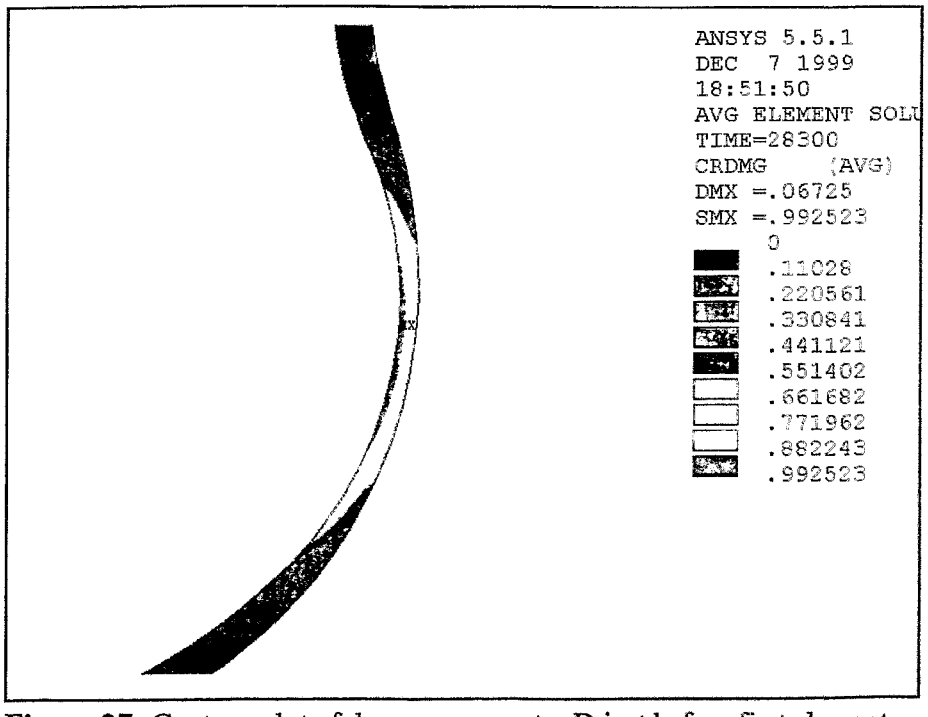

Figure 27: Contour plot of damage parameter D just before first element reaches D=1 and is killed (assumed fracture strain ε_{frac}=40%).

8 Summary and Outlook

In this report a short description of the phenomena occurring in the course of the FOREVER experiments is given. The combined modelling strategy of thermo-fluid-dynamic and structure mechanical Finite-Element calculations is described and an advanced numerical creep and damage parameter model is presented.

The post test calculations of the FOREVER-C2 experiment show that the behaviour of the vessel - made of French RPV steel - is quite sensitive to temperature variations during the creep deformation stage. Therefore, it appears that the unexpected deformation behaviour during the experiment is caused by the transient temperature field in the vessel wall rather than by a tertiary creep process.

The model will be improved by employing the transient thermal boundary conditions which have a great influence on the transient creep calculation. First rupture estimations have shown that one of the most important mechanical parameters of the material to be investigated in the future is the creep rupture strain.

References

ANSYS, 1998, Programmer's Manual. ANSYS, Inc.
Azodi, D., P. Eisert, U. Jendrich, W.M. Kuntze, 1996, GRS-Report GRS-A-2264.

Becker, A.A., Background to Material Non-Linear Benchmarks. NAFEMS-report R0049 (International Association for the Engineering Analysis Community).

Chu, T.Y., Pilch, M.M., Bentz, J.H., Ludwigsen, J.S., Lu, W.Y., Humphries, L.L., 1999, "Lower Head Failure Experiments and Analyses", Report, NUREG/CR-5582, SAND98-2047, Sandia National Laboratories, Albuqerque, NM, USA.

Ikonen, K., 1999, "Creep Model Fitting Derived from REVISA Creep, Tensile and Relaxation Measurements", Technical Report MOSES-4/99, VTT-Energy, Espoo, Finland.

James, A.M., Lord, M.P., 1992, "Macmillan´s Chemical and Physical Data", The Macmillan Press, London, GB.

Launder, B.E., Spalding, D.B., 1974, "The Numerical Computation of Turbulent Flows", Computer Methods in Applied Mechanics and Engineering 3, pp. 269-289.

Sehgal, B.R., Nourgaliev, R.R., Dinh, T.N., Karbojian, A., 1999, "FOREVER experimental program on reactor pressure vessel creep behavior and core debris retention", Proceedings of the 15-th International Conference on Structural Mechanics in Reactor Technology (SMiRT-15), Seoul, Korea, August 15-20, 1999.

Sehgal, B.R., Nourgaliev, R.R., Dinh, T.N., 1999, "Characterization of heat transfer processes in a melt pool convection and vessel-creep experiment", NURETH-9, San Francisco, Oct. 3-8, 1999.

Sala, A., 1984, "Radiant Properties of Materials, Tables of Radiant Values for Black Body and Real Materials", Elsevier, Amsterdam.

Verein Deutscher Ingenieure, 1994, "VDI-Wärmeatlas, Berechnungsblätter für den Wärmeübergang", 7. Auflage, VDI-Verlag, Düsseldorf, Germany.